

Determining the statistical significance of meteorite–asteroid pairs using geocentric parameters

P.M. Shober¹

Laboratoire Temps Espace, CNRS, Observatoire de Paris, PSL Université, Sorbonne Université, Université de Lille 1, UMR 8028 du CNRS, 77 av. Denfert-Rochereau 75014 Paris, France

Received June 7, 2025; accepted

ABSTRACT

Context. Orbital similarity between precisely observed meteorite falls and near-Earth asteroids (NEAs) has been presented for decades as evidence that some meteorites are coming directly from these asteroids. However, analysis of the statistical significance of these pairings is mixed. Based on osculating orbital elements, there is no evidence of statistically significant clustering; however, some analyses that account for secular perturbations suggest that streams are present.

Aims. We tested the statistical significance of meteorite-dropping fireballs and NEA clustering using the D_N similarity function based on four geocentric quantities (U , θ , ϕ , and λ_\odot).

Methods. We calculated the cumulative similarity found between 46 meteorite falls, 535 potential meteorite-dropping fireballs, and 20 516 NEAs maintained by NEODyS-2, along with 34 836 NEAs maintained by NASA/JPL HORIZONS. Statistical significance was estimated either by (1) using a kernel density estimation-based method to estimate the sporadic background distribution and thus draw random samples or (2) applying a uniform random solar longitude (λ_\odot). Each comparison to the synthetic sporadic population was repeated to estimate the 3σ region for which the cumulative similarity distribution is consistent with random association levels.

Results. The observed D_N cumulative similarity distribution of 46 instrumentally observed meteorite falls, 535 potential meteorite-dropping fireballs, and over 30k NEA radiants (estimated using six different radiant methods) reveals no statistically significant excess of similarity between the populations consistent with streams.

Conclusions. Based on nearly 600 fireball observations and geocentric impact parameters, we find there is no statistically significant clustering between meteorite falls and NEAs. If some meteorites arrive in streams, they make up less than $\sim 0.1\%$ of all falls. Recent asteroid or meteoroid physical processes could still explain features found in meteorites, but this activity is not producing distinguishable orbital streams or pairs.

Key words. Meteorites, meteors, meteoroids – Minor planets, asteroids: general – method: data analysis

1. Introduction

Meteor shower identification has relied heavily on ‘orbital similarity’ functions over the previous half century. These functions enable us to compare pairs of orbits and identify streams that stand out against the sporadic background population. Initially introduced by Southworth & Hawkins (1963), the D_{SH} value is derived by comparing two sets of orbital elements. This measure, which increases as the similarity decreases, is often termed a ‘dissimilarity parameter’. Several adaptations have been introduced, each slightly changing the degree of influence of different elements on the D value (Drummond 1981; Steel et al. 1991; Jopek 1993; Jopek et al. 2008; Jenniskens 2008). Although D criteria and other similarity metrics are widely employed, the results can be easily misinterpreted as the significance depends strongly on sample size, relative background flux, and the clustering algorithm chosen (e.g. single-linkage, DBSCAN, etc.; Jopek & Froeschlé 1997; Pauls & Gladman 2005; Koten et al. 2014; Egal et al. 2017; Jopek & Bronikowska 2017; Vida et al. 2018; Shober & Vaubaillon 2024; Jopek et al. 2024; Shober et al. 2025a). This is also heightened by the recent recognition that uncertainties in meteor- and fireball-based orbital elements are less precise than once believed (Egal et al. 2017; Vida et al. 2018; Shober et al. 2023). Several alternative similarity metrics and shower identification methods have also been introduced to overcome these shortcomings (Valsecchi et al. 1999; Jenniskens et al.

2009a; Brown et al. 2010; Peña-Asensio & Sánchez-Lozano 2024).

Many parent bodies have been identified¹ using similarity metrics in concurrence with complex numerical integrations of meteoroid streams. The parent bodies generally agreed upon within the scientific community are all related to larger, mostly cometary, meteor showers (Jenniskens 2006; Ďurišová et al. 2024). None of these well-established meteor showers have produced macroscopic meteorite samples, but some studies have explored this possibility (Brown et al. 2013). There have also been a plethora of studies examining the hypothesis that larger, meteorite-dropping fireballs could be associated with streams of material. Most notably, the proposed meteorite pairs of Innisfree–Ridgedale (Halliday 1987), Příbram–Neuschwanstein (Spurný et al. 2003), and Chelyabinsk–NEA 1999 NC43 (Borovička et al. 2013a) have all since been shown to be very likely not statistically significant pairings based solely on orbital similarity (Pauls & Gladman 2005; Koten et al. 2014; Reddy et al. 2015; Shober et al. 2025a). Several works have even proposed that a large portion of meteorites (up to over 50%) can be directly linked to near-Earth asteroids (NEAs) based on their orbits alone (e.g. Peña-Asensio et al. 2022; Hlobík & Tóth 2024). However, in these studies, either too large D criteria were

¹ <https://ceresiaumdc.ta3.sk/listofparents>

used or some other implicit assumptions caused the estimated statistical significance to be unreasonably high (Shober et al. 2025a). Clustering within the NEA population has been identified (Jopek 2020; Granvik & Walsh 2024; Shober et al. 2025a); however, no considerable statistical evidence to date supports associations between fireballs and such NEAs.

Nevertheless, the idea that NEAs could be the immediate precursor bodies of at least some meteorites on Earth and form debris streams is not unfounded (Borovička et al. 2015a). Recent work has identified statistically significant clustering amongst NEAs, likely linked to tidal disruptions during close encounters with the Earth (Jopek 2020; Granvik & Walsh 2024; Shober et al. 2025a). de la Fuente Marcos & De la Fuente Marcos (2016) also found that the distributions of ω and Ω deviate strongly from uniformity, with some groupings suggested to be due to streams, but most of the deviation observed is produced by secular and Kozai resonances rather than streams. Additionally, analysis of the meteoritic samples themselves, along with observations of recent asteroid activity, has bolstered recent interest in this concept (Lauretta et al. 2019; Turner et al. 2021; Scott & Herzog 2021; Shober et al. 2024; Jenniskens & Devillepoix 2025). Thus, searching for immediate precursor bodies of meteorite falls amongst NEAs is worthwhile.

A recent re-analysis of the ‘decoherence lifetimes’ of near-Earth meteoroid streams and the statistical significance of clustering amongst meteorite-dropping fireballs and NEAs found no evidence to support the dozens of claims made over the previous two decades that meteorites can be directly linked to NEAs using their orbits (Shober et al. 2025a). However, this study only examined three separate orbital similarity functions (Southworth & Hawkins 1963; Drummond 1981; Jopek 1993) using the osculating orbital elements at the observation epoch of the fall.

The dynamical ‘decoherence’ of meteoroid streams (i.e. the time that it takes for a stream to become indistinguishable from the sporadic background) is usually around $\sim 10\text{--}50$ kyr for minor streams near the Earth (Pauls & Gladman 2005; Shober et al. 2025a). However, during this period, the secular precession of the argument of perihelion (ω) cycles an NEA through a sequence of discrete Earth-intersection geometries. A single orbit can cross the Earth four times per ω cycle (quadruple crossers) or up to eight times for highly inclined cases, generating multiple distinct geocentric radiants (Gronchi & Milani 2001; Babadzhanov et al. 2012; Pokorný & Vokrouhlický 2013). Any fragments ejected within the past few tens of millennia could impact Earth at radiants that bear little resemblance to the present-day orbit of the immediate-precursor body. The practical consequence is that searches confined to a meteorite’s current radiant risk missing earlier intersections elsewhere in the cycle. This mechanism underpins the well-studied 96P/Machholz complex and other stream complexes (Babadzhanov 2001; Babadzhanov et al. 2008; Neslušan et al. 2013; Neslušan & Hajduková 2014; Babadzhanov et al. 2015, 2017; Kholshevnikov et al. 2016; Neslušan & Hajduková 2021).

Carbognani & Fenucci (2023) sampled the entire ω cycle for 16 227 NEAs, finding 30 740 possible impact radiants; they determined that 20 of the 38 instrumentally observed meteorites can be paired with specific NEAs. However, their significance assessment relied on a single random trial and no formal confidence limits. Here, we build upon the results of Shober et al. (2025a) and extend the analysis of Carbognani & Fenucci (2023). While no statistically significant meteorite-dropping streams are observed at the current epoch, it is necessary to test whether these statistically significant associations

can be found when searching all possible NEA radiants during their secular ω cycle.

2. Data

We used data from 46 instrumentally observed recovered meteorite falls along with 535 possible meteorite falls. The 535 possible falls were observed by the Global Fireball Observatory (GFO²; Devillepoix et al. 2020), the European Fireball Network (EFN; Borovička et al. 2022b,a), or the Fireball Recovery and InterPlanetary Observation Network (FRIPO³; Colas et al. 2020). The possible falls were identified using the α - β criterion (Sansom et al. 2019) for GFO and FRIPO³ observations, with a minimal final mass of at least 1 g and $\geq 20\%$ atmospheric deceleration. The EFN possible meteorite-dropping subset was identified in Borovička et al. (2022b). For further information about the data, please refer to the Methods section of Shober et al. (2025b), from which these data were taken. The 46 meteorite falls used can be found in A.1.

3. Methods

3.1. D_N criterion

Classical D parameters compare two orbits in the five-element heliocentric space (a , e , i , Ω , and ω), but that strategy suffers from two fundamental drawbacks. First, a meteor’s heliocentric elements are derived from a short fireball arc and are far less precise than those of asteroids. Second, those elements evolve on $10^3\text{--}10^5$ yr timescales under planetary perturbations, so a small D value measured today is not, by itself, proof of common origin (Pauls & Gladman 2005; Babadzhanov et al. 2012; Pokorný & Vokrouhlický 2013; Babadzhanov et al. 2015, 2017; Shober et al. 2025a). To bypass these limitations, Valsecchi et al. (1999) introduced the distance function D_N , defined in a space of four geocentric observables that are directly derived from the observations (unlike orbital elements) and thus matched to the actual dimensionality of a well-observed fireball. The four coordinates are the magnitude of the unperturbed geocentric velocity (U), the two Öpik encounter angles (θ and ϕ), which specify the direction of U after removing Earth’s gravitational deflection, and the solar longitude at impact (λ_\odot).

The similarity criterion, D_N , is defined as

$$D_N^2 = (U_2 - U_1)^2 + w_1(\cos \theta_2 - \cos \theta_1)^2 + \Delta\xi^2, \quad (1)$$

where

$$\Delta\xi^2 = \min(w_2\Delta\phi_I^2 + w_3\Delta\lambda_I^2, w_2\Delta\phi_2^2 + w_3\Delta\lambda_2^2) \quad (3)$$

$$\Delta\phi_I = 2 \sin\left(\frac{\phi_2 - \phi_1}{2}\right) \quad (4)$$

$$\Delta\phi_2 = 2 \sin\left(\frac{180^\circ - \phi_2 - \phi_1}{2}\right) \quad (5)$$

$$\Delta\lambda_1 = 2 \sin\left(\frac{\lambda_2 - \lambda_1}{2}\right) \quad (6)$$

$$\Delta\lambda_2 = 2 \sin\left(\frac{180^\circ - \lambda_2 - \lambda_1}{2}\right), \quad (7)$$

and w_1 , w_2 , and w_3 are suitably defined weighting factors. All weightings were set to 1.0 here, as this is standard practice and was originally used in Jopek et al. 1999. Note that $\Delta\xi$ is small if $\phi_1 - \phi_2$ and $\lambda_1 - \lambda_2$ are either both small or both close to 180° .

² <https://gfo.rocks/>

³ <https://www.fripo.org/>

3.2. NEA radiant methods

To replicate the analysis of Carbognani & Fenucci (2023), this analysis also uses the list of NEA geocentric encounter conditions U , θ , ϕ , and λ_\odot maintained by NEODYs-2⁴. This list was computed with the ORBFIT software⁵ that gives the encounter conditions for 20 516 NEAs of the total 86 946 possible radiants. Carbognani & Fenucci (2023) used radiants from only 16 227 NEAs; otherwise, the methodology of the analysis is identical.

To confirm that the results are not tied to a specific orbit-to-radiant conversion, we augmented the NEODYs/ORBFIT set with five additional theoretical radiant lists generated by the B, A, W, H, Q algorithms in Neslušan's program (Neslušan et al. 1998). These routines all force an orbit to cross Earth's path but differ in which elements are minimally adjusted: (i) in the Q (perihelion-shift) method, only q is varied (Hasegawa 1990); (ii) the B method shifts both q and e (Svoren et al. 1993); (iii) the W method rotates the line of apsides (ω shift) (Steel & Bagley 1985); (iv) the A method rotates the orbit about the apsidal line (Svoren et al. 1993); and (v) the H method simultaneously tweaks ω and i (Hasegawa 1990).

Radiants were computed for all 34 836 NEAs whose osculating elements are archived in the Jet Propulsion Laboratory (JPL) HORIZONS system⁶ – a dataset more than twice the size used by Carbognani & Fenucci (2023). By analysing the D_N statistics derived from the six independent radiant sets, we can test whether any meteorite–NEA pairing is robust to both the choice of radiant algorithm and the inclusion of a more complete NEA catalogue.

3.3. Estimating sporadic distributions

Two methods were used to estimate the sporadic background population and test the statistical significance of observed clustering. To replicate the Carbognani & Fenucci (2023) methodology, we kept the NEODYs/ORBFIT parameters (U , θ , and ϕ) of every NEA and meteorite-dropping fireball fixed but replaced λ_\odot with a value drawn from a uniform distribution between 0° and 360° . This effectively randomises the date of the encounter with the Earth. This randomisation must be done for both NEA radiant and fireball populations, as the null hypothesis under consideration is that both fireball and NEA geocentric parameters are sporadic. Carbognani & Fenucci (2023) only randomised the λ_\odot for the NEA population; however, this implicitly assumes that the meteorite geocentric parameters are not clustered. If this is not true, i.e. there are streams, any real streams within the observed dataset could have their statistical significance mischaracterised because they were assumed to be sporadic in the null test. A similar method was used by Pauls & Gladman (2005), except they randomised the Ω of the samples.

Furthermore, although randomising the orientations, either λ_\odot or Ω , has been previously used to estimate sporadic distributions, they assume uniform distributions that are not consistent with actual sporadic observations (see Fig. 1 or 2). The sporadic distribution of meteoroids and asteroids do not have uniform λ_\odot or Ω distributions (JeongAhn & Malhotra 2014), and the observed populations have observational biases that further skew the distributions (Halliday et al. 1996; Granvik et al. 2018). Seasonal effects, resonances, and observational biases change and

modify these distributions. If the biases are not present, the expected degree of similarity between the populations will drop precipitously. For example, in Hlobík & Tóth (2024), they drew random samples from the de-biased near-Earth object (NEO) model of Granvik et al. (2018) and compared them to the orbits of recovered meteorites. This is fatally flawed, as the populations being compared are not the same as the populations being tested. The distribution of known NEOs exhibits significant observational biases, resulting in a greater overall similarity within the population compared to the terrestrial impact populations. Thus, it is critical to test the degree of similarity expected for the sporadic observed populations. Otherwise, deviations in the amount of similarity could appear that are unrelated to the problem of statistically significant meteorite–NEA streams.

We also modelled the sporadic background for both the meteorite-fall and NEA-radiant populations with kernel density estimation (KDE; Vida et al. 2017; Shober & Vaubaillon 2024). The probability density function (PDF) output based on the 535 possible meteorite falls was also used to generate random samples for the 46 recovered meteorites. A KDE places a smooth kernel, here a multivariate Gaussian, on every data point and sums those kernels to obtain a continuous estimate of the underlying PDF. Unlike a histogram, KDE is non-parametric, free of arbitrary bin edges, and is one of the most effective methods for generating realistic synthetic samples (Vida et al. 2017; Shober & Vaubaillon 2024). One can draw arbitrarily large Monte Carlo samples from it, obtaining synthetic radiants that preserve the full covariance structure of the original data while seamlessly smoothing out any remaining minor clusters, precisely the behavior desired for significance testing. However, it is essential to note that while this approach is seen as an improvement over simply randomising the impact date, it is extremely easy to obtain unrealistic results if the parameters are not rigorously inspected to be realistic (i.e. within the correct range, maintaining the cyclic nature of angles, etc.). In this study, after Z-score standardisation of the data, we transformed the three cyclic angles (λ_\odot , θ , and ϕ) to Cartesian pairs ($\cos \alpha$ and $\sin \alpha$), ensuring circular continuity and the full covariance structure of the data in the seven-dimensional space ($\cos \lambda_\odot$, $\sin \lambda_\odot$, $\cos \theta$, $\sin \theta$, $\cos \phi$, $\sin \phi$, and U). A diagonal, anisotropic Gaussian kernel was fitted with bandwidths h_i obtained from the improved Sheather–Jones (ISJ) estimator (Sheather & Jones 1991; Botev et al. 2010); this automatically balances over- and under-smoothing across dimensions while retaining inter-parameter correlations. The mean integrated squared error (MISE) gauges the accuracy of a kernel-density estimate $\hat{f}(x; h)$,

$$\text{MISE}(h) = \mathbb{E} \left[\int (\hat{f}(x; h) - f(x))^2 dx \right], \quad (8)$$

where h is the kernel bandwidth. In practical terms, h sets the trade-off between noise and smoothing: narrow kernels follow every bump in the data but amplify noise, whereas wide kernels smooth noise at the cost of erasing real structure. ISJ chooses the bandwidth that minimises the large-sample limit of the asymptotic MISE (AMISE). The AMISE depends on the ‘roughness’ of the true density, $\|f''\|^2$, a quantity that cannot be measured directly, so the ISJ algorithm estimates that roughness from the data in a self-consistent, recursive fashion (Botev et al. 2010). The bandwidth returned by ISJ is therefore the one that minimises the expected squared difference between the KDE and the true, but unseen, density, yielding a smoothing level that retains genuine orbital structure while filtering out sampling noise. ISJ is ideal for orbital or radiant distributions, as they can be multimodal and generally not normally distributed.

⁴ <https://newton.spacedys.com/~neodys2/propneo/encounter.cond>

⁵ <http://adams.dm.unipi.it/orbfit/>

⁶ <https://ssd.jpl.nasa.gov/horizons>

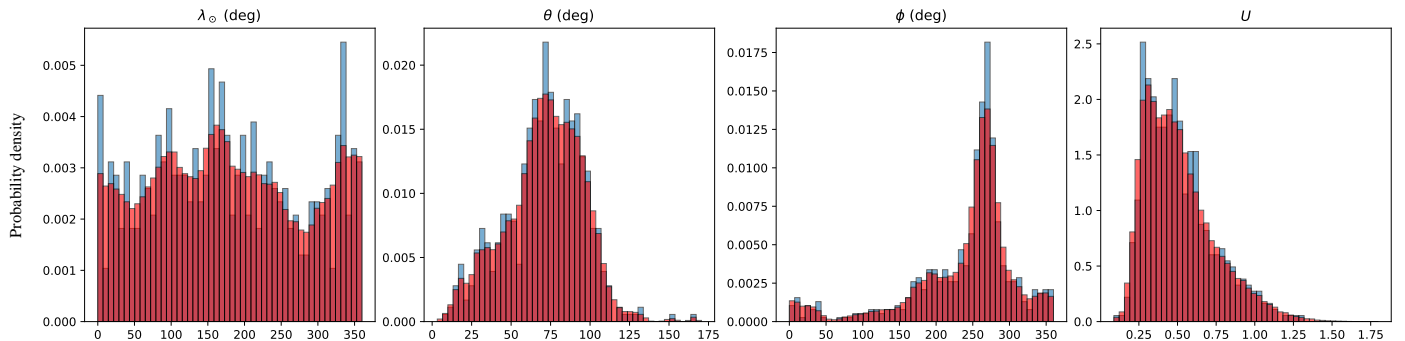


Fig. 1: Geocentric parameter distribution of 535 potential meteorite-dropping fireballs (blue) versus the KDE-estimated PDF (red) using a Gaussian kernel with a bandwidth of [0.2564, 0.2564, 0.2489, 0.2564, 0.1619, 0.2333, 0.2564]. This PDF, which approximates the corresponding observed sporadic population, was used to estimate the degree of random association in the population through Monte Carlo simulations.

3.4. Statistical significance

To assess the statistical significance of any excesses of similarity based on D_N , a methodology similar to that of Shober et al. (2025a) was used. Monte Carlo experiments were conducted where $N_{\text{population}}$ draws, equal in size to the original datasets, were randomly generated from our sporadic background distribution estimates (as described in Sect. 3.3). The D_N value was then calculated for every possible pair combination between the sporadic meteorite-dropping fireball population and sporadic NEA radiant population. The cumulative similarity distribution (CSD), which describes the total number of pairs that are $< D_N$ as a function of D_N , was estimated for the 46 recovered meteorites and each of the six radiant methods described in Sect. 3.2. Additionally, the CSDs of the 535 possible falls and the six different NEA radiant distributions were also calculated. In total, we tested the statistical significance of 12 different CSDs to determine whether a statistically significant amount of similarity exists among the 46 recovered falls or the 535 fireballs, based on geocentric parameters. This was then carried out ten times for each CSD to estimate the 3σ confidence region, which describes the amount of similarity expected within the population due to random associations. If an ongoing mechanism were truly creating meteoroid streams in near-Earth space, the distribution of D_N values would show a marked surplus at the low end of the CSD distribution, a deviation from a power law (Vokrouhlický & Nesvorný 2008; Rozek et al. 2011; Shober et al. 2025a). Using synthetic sporadics generated with the randomised λ_0 or the KDE-based Monte Carlo tests, we evaluated D_N for more than 7×10^8 unique combinations.

4. Results

4.1. Kernel density estimates of the sporadic background

A multivariate Gaussian KDE was fitted to each radiant sample (Fig. 1 for the 535 potential falls; Fig. 2 for the six NEA catalogues). Figure 1 shows that the resulting meteorite fall PDF reproduces the seasonal modulation in λ_0 produced mainly by weather and radiant-visibility biases. Non-negligible non-uniformities appear in the NEA radiants as well (Fig. 2), which are expected and consistent with the results of JeongAhn & Malhotra (2014). These red regions are the PDFs from which all Monte Carlo ‘sporadic’ samples were drawn. For comparison, we also generated control samples by holding (U, θ, ϕ) fixed

and assigning a uniformly random λ_0 , as done in Carbognani & Fenucci (2023).

Method-dependent differences are evident in the fitted radiant PDFs (Fig. 2), reflecting how each algorithm enforces Earth intersection. In particular, Method A (rotation about the apsidal line; Svoren et al. 1993) reorients the orbital plane by changing (i, Ω) while leaving (q, e, ω) fixed, which drives the asymptotic geocentric approach azimuth to cluster at $\phi \simeq 0^\circ$ and 180° . In contrast, the Q/B/W/H variants modify q, e , or rotate the line of apsides (ω) while leaving the plane orientation (i, Ω) unchanged or only weakly perturbed, thereby shifting the Earth-intersection to different true anomalies within an essentially fixed plane and yielding mutually similar ϕ distributions that lack the $0^\circ/180^\circ$ concentration characteristic of Method A (often with excess near $90^\circ/270^\circ$). The standard-scaled ISJ bandwidths are listed in Table 1.

4.2. Cumulative similarity statistical significance

Figures 3 and 4 present the main test of this work: the CSDs of D_N for (i) the 46 recovered falls and (ii) the 535 potential >1 g falls, each compared against six independent NEA radiant catalogues (one per panel). In every panel, the red curve (labelled ‘Actual data’) is the empirical cumulative count of all possible fall-radiant pairs with D_N below a threshold. The two shaded regions represent the expected range of values for random associations using two different methods: the blue region is the 3σ range from Monte Carlo draws of the KDE-modelled sporadic background (Sect. 3.3), and the red region is the 3σ range from samples with uniformly randomised λ_0 . The interpretation is straightforward: a statistically significant stream-like excess would manifest as the ‘actual data’ curve deviating from a power law and rising above both the 3σ blue and red regions, particularly at low D_N . Small differences among panels are expected because each radiant method enforces Earth intersection via different element adjustments (Sect. 3.2).

Carbognani & Fenucci (2023) argued that 82% of meteorite-NEA pairs with $D_N < 0.06$ should be genuine. Using their NEODyS/ORBFIT radiants, we were able to reproduce all pairs listed in their Table 3. The observed CSD (red curve in Fig. 3) sits above their black curve by a constant offset. This vertical shift is entirely explained by the additional ~ 4300 Earth-crossing NEAs included here (20516 versus 16227); once normalised, the two CSDs coincide. The expected amount of stochastic similarity between the NEODyS/ORBFIT radiants

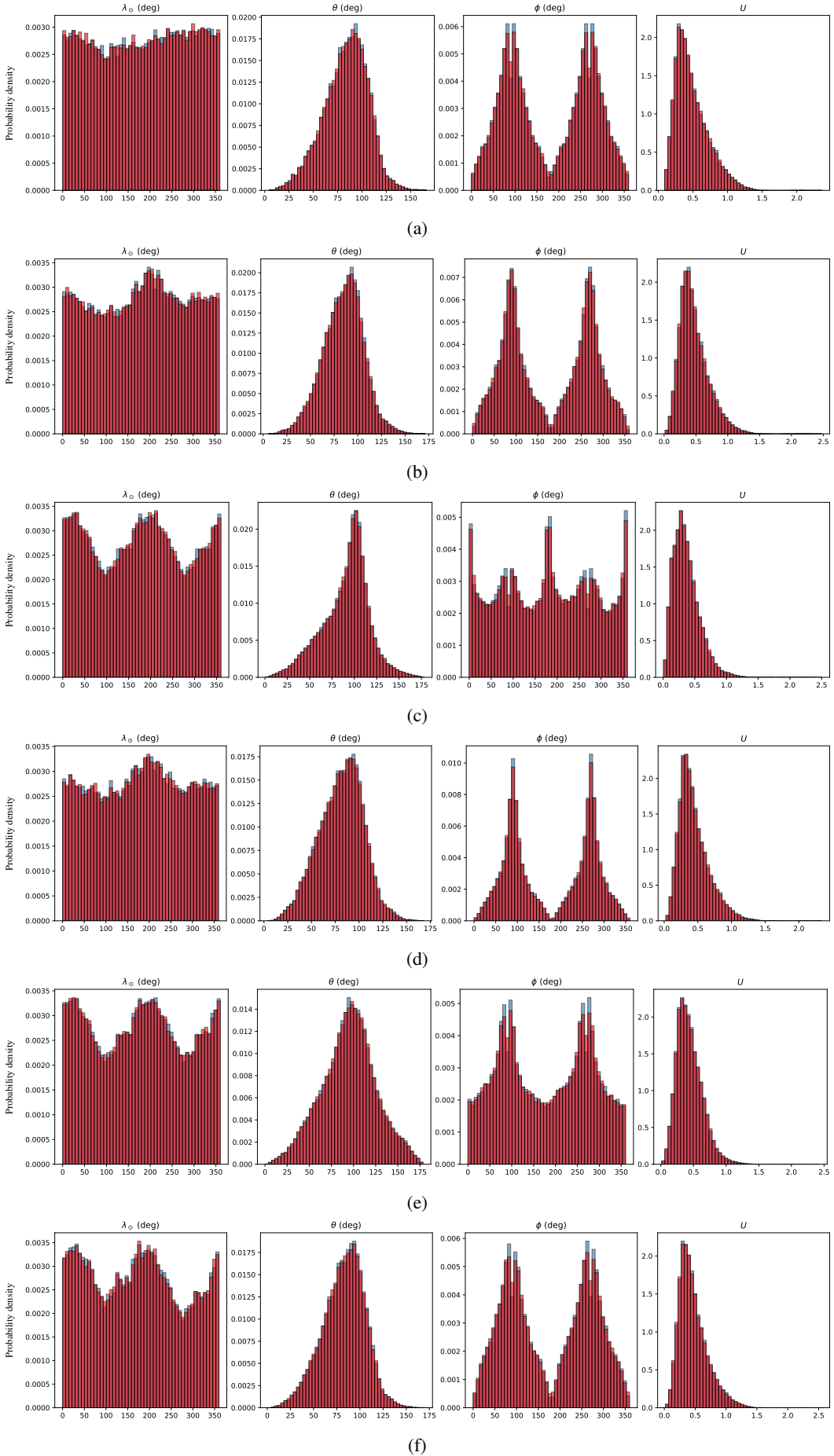


Fig. 2: Geocentric parameter distribution of estimated NEA radiants (blue) versus the KDE-estimated PDF (red) using a Gaussian kernel: NEODyS-2 (a), Method A (b), Method B (c), Method H (d), Method Q (e), and Method W (f). These PDFs were used to estimate the degree of random association in the population through Monte Carlo simulations.

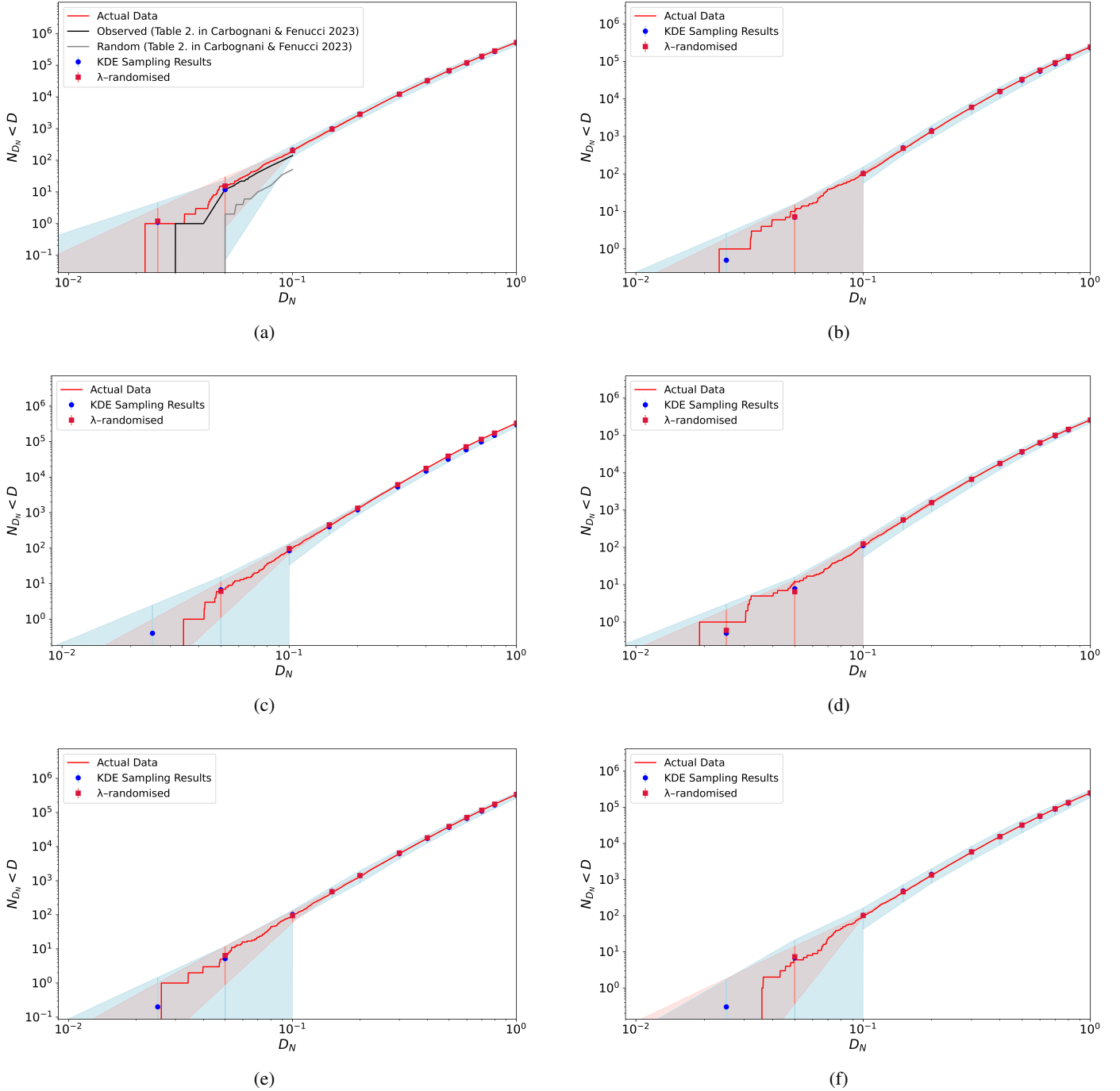


Fig. 3: CSDs of the 46 recovered meteorite falls and NEA theoretical impact radiants: NEODYs-2 (a), Method A (b), Method B (c), Method H (d), Method Q (e), and Method W (f). The red curve, labelled ‘Actual Data’, represents the cumulative similarity between every possible radiant–fall pair combination for the 46 falls and the theoretical NEA radiants of a particular method. The NEA radiants were estimated using six different methods, one for each panel. Two sporadic association regions are estimated. The blue region encompasses the 3σ confidence region for random associations based on the KDE-drawn samples. The red region represents the 3σ confidence region for random associations based on a uniformly random λ_{\odot} . In panel (a), the ‘observed’ and ‘random’ curves reported by Carbognani & Fenucci (2023) are also included for comparison purposes.

and 46 recovered meteorites is estimated by (i) randomising only λ_{\odot} as in Carbognani & Fenucci (2023) (red region) and (ii) the KDE synthetic sporadic background introduced in Sect. 3.3 (blue region). The observed CSD never exceeds the 3σ expectation envelope (Figs. 3a–f), i.e. the amount of similarity between the NEA population and the 46 recovered falls is completely consistent with levels expected due to random associations. The

single, marginal excursion for method H at $D_N \approx 0.02$ remains well within the spread imposed by fireball radiant-velocity uncertainties and therefore is not significant.

Additionally, for random points in a d -dimensional space, the theoretical CSD follows a power law where $N(< D) \propto D^d$; asteroid-pair studies using five osculating elements indeed find slopes $\alpha \approx 4.7$ (Vokrouhlický & Nesvorný 2008). D_N is built

Table 1: ISJ bandwidth vectors (standard-score space).

Sample	h_{sol_x}	h_{θ_x}	h_{ϕ_x}	h_{sol_y}	h_{θ_y}	h_{ϕ_y}	h_U
535 potential falls	0.256	0.256	0.249	0.256	0.162	0.233	0.256
46 recovered falls	0.423	0.402	0.423	0.423	0.209	0.423	0.299
NEODyS/ORBFIT	0.0926	0.0926	0.0926	0.0926	0.0539	0.0926	0.0926
Method A	0.109	0.109	0.109	0.109	0.0653	0.109	0.105
Method B	0.0968	0.0966	0.0968	0.0968	0.0556	0.0968	0.0918
Method H	0.108	0.108	0.0996	0.108	0.0723	0.108	0.106
Method Q	0.0968	0.0968	0.0968	0.0968	0.0720	0.0968	0.0946
Method W	0.108	0.108	0.108	0.108	0.0636	0.108	0.106

from four geocentric parameters, and thus the expected index drops to $\alpha \approx 4$. A linear least-squares fit to our observed CSDs across the six radiant catalogues yields $\alpha = 3.75\text{--}3.88$ (except Method Q, where $\alpha \simeq 4.35$) with uncertainties of 0.21–0.30, all statistically consistent with $\alpha_{\text{th}} = 4$. These uncertainties were estimated by a 2,000-sample parametric bootstrap of the per-bin increments and by taking half the spread of slopes when varying the upper fit bound $D_N^{\text{max}} \in [0.08, 0.12]$; the quoted σ combines the two in quadrature. The slightly shallower slope obtained from a broader fit (our nominal $\alpha \simeq 3.8$) likely reflects finite-range effects and mild metric non-linearity in D_N . In contrast, the grey ‘random’ line plotted by Carbognani & Fenucci (2023) is an order of magnitude too low and, by construction (because it represents random associations), should be strictly linear; implying potentially a numerical error rather than a physical signal. Additionally, the grey ‘random’ curve is only one sampling by Carbognani & Fenucci (2023), and does not encapsulate the confidence region but rather just one single estimate, which can vary significantly as we do not know the true sporadic population, especially when only based on 38 falls.

Similarly, as seen in Fig. 4, the CSD analysis for the 535 fireballs that satisfy the $m \geq 1\text{ g}$ and 20% deceleration criterion, does not show evidence of statistically significant clustering at low D_N values. Every red curve sits comfortably inside the blue (KDE) and red (random- λ_{\odot}) 3σ regions. Thus, even when the meteorite-dropping sample is an order of magnitude larger, there is still no clear evidence of recently formed meteorite-dropping streams.

A mild systematic offset appears at $D_N \sim 0.1$ in the NEODyS/ORBFIT panel (Fig. 4a), where the observed CSD rises above the KDE envelope but not the randomised λ_{\odot} . The same minor feature is present, though entirely contained within 3σ , for the analogous W-method based on 34 836 NEAs. In no case does the observed CSD fall outside both 3σ regions; thus, this is likely a shortcoming of the KDE smoothing in this instance. In short, none of the six catalogues shows the low- D_N surplus required for a detection, defined here as the ‘Actual data’ curve rising above the 3σ envelopes of both null backgrounds at small D_N . This non-detection implies that any detectable fall–NEA stream component is at most of order $\sim 10^{-3}$ of all falls (i.e. a larger contribution would have produced a visible excess). This is a detectability limit for our CSD test, not a formal binomial bound on the underlying fraction; for reference, a one-sided 3σ upper limit with zero detections in $N=535$ falls is $\lesssim 0.5\%$. Streams of the order of the $\sim 10^{-3}$ level may exist but would be below the sensitivity of the present analysis.

5. Discussion

Analysis of 46 recovered meteorites and 535 possible $\geq 1\text{ g}$ meteorite-dropping fireballs shows that the CSDs all follow an almost perfect power law at small D_N values, enclosed by the

3σ envelopes expected for random pairings (Figs. 3 and 4). In other words, the amount of similarity found between the NEA geocentric radiants and the meteorite-dropping fireballs is fully consistent with that expected due to random associations. There are two instances where the observed CSDs step outside a single 3σ envelope (Figs. 3d and 4a), but neither satisfies our detection criterion (a low- D_N surplus above both null envelopes). In the 46-fall case, the excursion occurs only against the λ_{\odot} -randomised null and disappears once the reported meteor radiant and velocity uncertainties are propagated through the CSD, as those uncertainties smear low- D_N pairs and reduce any apparent excess. In the 535-fall NEODyS/ORBFIT panel, the modest rise above the KDE envelope occurs near $D_N \sim 0.1$, is not seen in the other five radiant catalogues (including the similar W method), and is therefore most likely a local KDE-smoothing artefact rather than a coherent stream signal. Taken together, these checks show no low- D_N surplus consistent with a recently formed, detectable stream.

There are two instances where the observed CSDs step outside a single 3σ envelope (Fig. 3d; Fig. 4a), but neither satisfies our detection criterion (a low- D_N surplus above both null envelopes). In the 46-fall case, the excursion occurs only against the λ_{\odot} -randomised null and disappears once the reported meteor radiant/velocity uncertainties are propagated through the CSD, as those uncertainties smear low- D_N pairs and reduce any apparent excess. In the 535-fall NEODyS/ORBFIT panel, the modest rise above the KDE envelope occurs near $D_N \sim 0.1$, is not seen in the other five radiant catalogues (including the similar W-method), and is therefore most likely a local KDE-smoothing artefact rather than a coherent stream signal. Taken together, these checks show no low- D_N surplus consistent with a recently formed, detectable stream.

From the widths of the 3σ envelopes at the smallest accessible separations, we inferred an order-of-magnitude detectability limit: any stream component contributing $\gtrsim 10^{-2}$ of all falls would produce a low- D_N surplus that rises above null regions; since no such excess is seen in any catalogue, the stream fraction is $\lesssim 10^{-3}$ if present. This limit is consistent with Shober et al. (2025a), who, using the classical D_{SH} , D' , and D_H orbital similarity criteria applied to osculating elements, found no statistically significant meteorite streams amongst meteorite dropping fireballs. The present analysis extends that test through an entire secular cycle for every NEA radiant and still uncovers no hidden concentrations. Even if every tidally generated NEA cluster contributed meteorite-sized fragments, the stream fraction would rise only to the $\simeq 0.2\%$, an upper bound estimated by Shober et al. (2025b) presuming complete overlap between the identified NEA clusters of Shober et al. (2025a) and the 535 potential fall dataset.

It is important to note that, within clustering studies like this one, the implicit assumption is that the broad features observed in our sporadic distribution are not related to streams. If some-

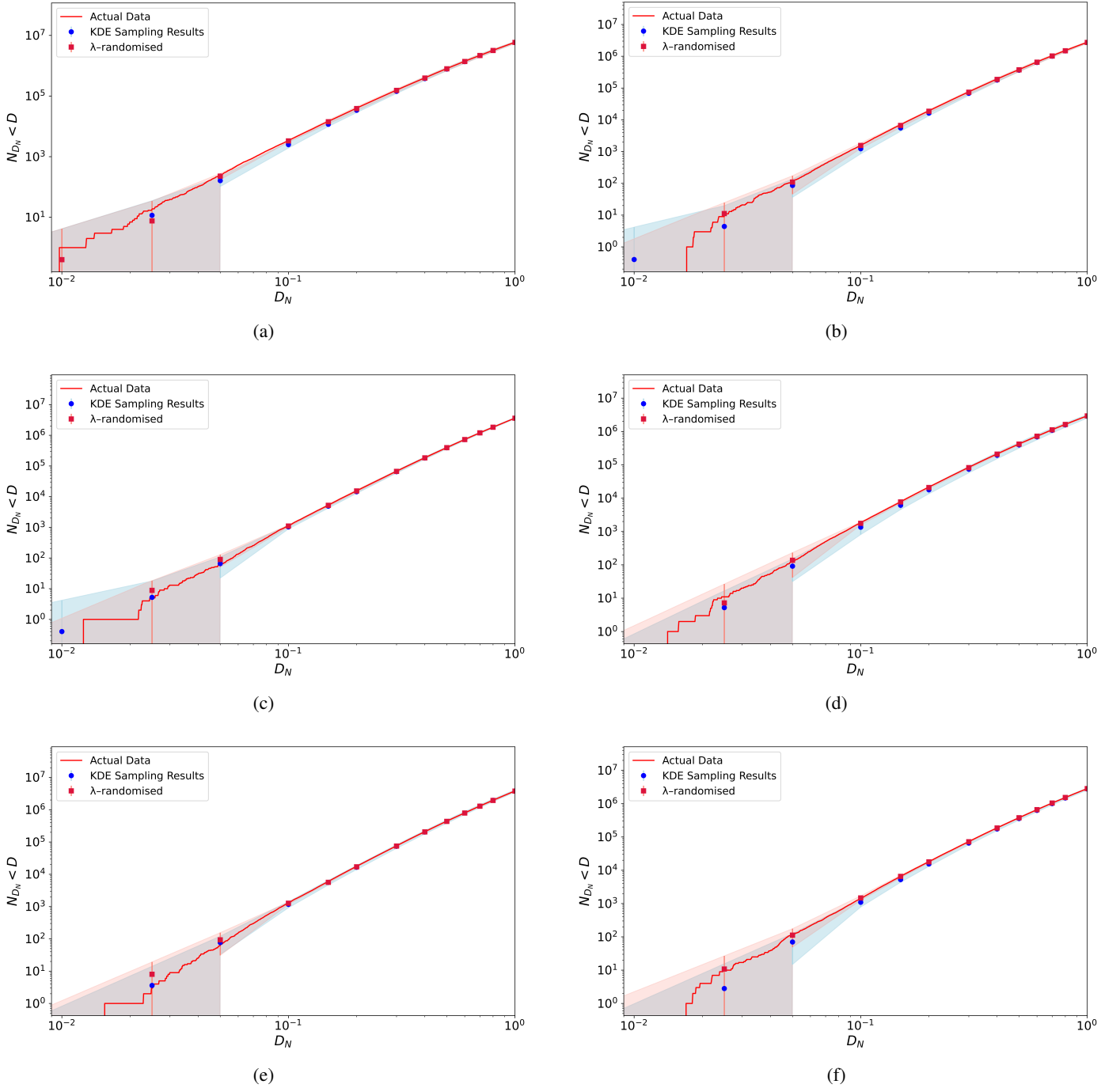


Fig. 4: Same as Fig. 3 but for 535 potential meteorite falls > 1 g observed by GFO, FRIPON, or FRIPON sensors and NEA theoretical impact radians.

one would like to make the argument that, still, many meteorites are related to NEAs and that these broad features are actually indicative of a recent meteoroid stream activity, they would have to show that the orbital distribution expected for larger meteoroids in near-Earth space is not consistent with the orbital distribution expected purely based on the relative abundances coming from different source asteroid families in the main belt. Recent work indicates the opposite: Brož et al. (2024b) found that most meteorites in our collections today originate from younger asteroid families, and their meteoroid transfer model called ME-

TEOMOD⁷ reproduces the principal features of the observed FRIPON fireball velocity distribution (see Fig. 12 in Brož et al. 2024a). Thus, the main, large-scale features of the fall population can be explained without invoking a substantial contribution from detectable streams of recently released material. Differences that remain are consistent with physical processing (e.g. thermal fragmentation during low-perihelion phases) rather than with a dominant stream component (Shober et al. 2025b).

There is significant evidence to suggest recent modification and activity within the near-Earth meteoroid and asteroid pop-

⁷ <https://sirrah.troja.mff.cuni.cz/~mira/meteomod/>

ulations (Borovička et al. 2015a; Granvik et al. 2016; Lauretta et al. 2019; Bottke et al. 2020; Wiegert et al. 2020; Turner et al. 2021; Scott & Herzog 2021; Shober et al. 2024; Granvik & Walsh 2024; Shober et al. 2025b; Jenniskens & Devillepoix 2025). However, this activity does not form large meteorite-dropping streams (Shober et al. 2025a; Chow & Brown 2025, and this work). Recent activity can generally modify the orbital distribution of meteoroids, but direct identification of immediate precursor asteroids for meteorites seems unlikely and would necessitate other compositional or physical constraints in addition to dynamical justifications to make a convincing argument in the future.

6. Conclusions

We investigated whether instrumentally observed meteorite falls or meteorite-dropping fireballs form statistically significant streams with NEAs when similarity is evaluated in four-dimensional geocentric space (U, θ, ϕ , and λ_\odot) using the D_N criterion (Valsecchi et al. 1999). We compared 46 recovered meteorites and 535 candidate meteorite-dropping fireballs to six theoretical NEA geocentric radiant catalogues, based on $> 30\,000$ NEOs. For each pairing, we built CSDs and benchmarked them against 10^7 – 10^8 Monte Carlo trials drawn from (i) a uniform λ_\odot distribution and (ii) kernel density estimates of the observed sporadic background. Our main results are:

1. None of the six impact radiant catalogues exhibits the low- D_N surplus required for a detection, i.e. the observed cumulative similarity curve never rises above the 3σ envelopes of both null backgrounds at small D_N . All 46-fall CSDs lie entirely within the expected bands, and the 535 potential fall set shows only a single, likely method-specific fluctuation near $D_N \sim 0.1$ that is absent in the other catalogues and remains inside the alternate null's 3σ envelope. We therefore find no evidence of meteorite–NEA streams. The fitted small- D_N slope, $\alpha = 3.8 \pm 0.25$, is also consistent with the $N(< D) \propto D^4$ behaviour expected for a stochastic four-dimensional population.

2. The upper limit on any hidden stream component is, therefore, at most $\sim 0.1\%$ of all known meteorite falls. Extending the search through the full secular precession cycle of each NEA does not reveal additional pairings.

3. These findings do not rule out recent physical activity (collisions, tidal disruption, thermal fragmentation, etc.) in the NEA population. Such processes are well documented, but studies show that this activity does not generate coherent, meteorite-dropping streams.

In short, geocentric-parameter clustering provides no evidence that a substantial fraction of meteorites arrive from contemporary NEA streams. Any future attempt to link individual meteorites to immediate-precursor NEAs will require considerable additional constraints beyond simple orbital similarity.

Acknowledgements. This project has received funding from the European Union's Horizon 2020 research and innovation programme under the Marie Skłodowska-Curie grant agreement No945298 ParisRegionFP. The Global Fireball Observatory and data pipeline is enabled by the support of the Australian Research Council (DP230100301, LE170100106). FRIPON was initiated by funding from ANR (grant N.13-BS05-0009-03), carried by the Paris Observatory, Muséum National d'Histoire Naturelle, Paris-Saclay University and Institut Pythéas (LAM-CEREGE). VigieCiel was part of the 65 Millions d'Observateurs project, carried by the Muséum National d'Histoire Naturelle and funded by the French Investissements d'Avenir program. FRIPON data are hosted and processed at Institut Pythéas SIP (Service Informatique Pythéas), and a mirror is hosted at IMCCE (Institut de Mécanique Céleste et de Calcul des Éphémérides / Paris Observatory). This research used Astropy, a community-developed core Python package for Astronomy (Robitaille et al. 2013).

References

Andrade, M., Docobo, J. Á., García-Guinea, J., et al. 2023, MNRAS, 518, 3850
 Babadzhanov, P. 2001, A&A, 373, 329
 Babadzhanov, P., Kokhirova, G., & Obrubov, Y. V. 2015, Sol. Syst. Res., 49, 165
 Babadzhanov, P., Kokhirova, G., Williams, I., & Obrubov, Y. V. 2017, A&A, 598, A94
 Babadzhanov, P., Williams, I., & Kokhirova, G. 2008, MNRAS, 386, 2271
 Babadzhanov, P., Williams, I., & Kokhirova, G. 2012, MNRAS, 420, 2546
 Bland, P. A., Spurný, P., Towner, M. C., et al. 2009, Science, 325, 1525
 Borovička, J., Bettonvil, F., Baumgarten, G., et al. 2021, Meteorit. Planet. Sci., 56, 425
 Borovička, J. & Kalenda, P. 2003, Meteorit. Planet. Sci., 38, 1023
 Borovička, J., Popova, O., & Spurný, P. 2019, Meteorit. Planet. Sci., 54, 1024
 Borovička, J., Spurný, P., & Brown, P. 2015a, Asteroids IV, 257
 Borovička, J., Spurný, P., Brown, P., et al. 2013a, Nature, 503, 235
 Borovička, J., Spurný, P., Šegon, D., et al. 2015b, Meteorit. Planet. Sci., 50, 1244
 Borovička, J., Spurný, P., & Shrbený, L. 2022a, A&A, 667, A158
 Borovička, J., Spurný, P., Shrbený, L., et al. 2022b, A&A, 667, A157
 Borovička, J., Tóth, J., Igaz, A., et al. 2013b, Meteorit. Planet. Sci., 48, 1757
 Botev, Z. I., Grotowski, J. F., & Kroese, D. P. 2010
 Bottke, W., Moorhead, A., Connolly Jr, H., et al. 2020, J. Geophys. Res. Planets, 125, e2019JE006282
 Brown, P., Cephecha, Z., Hawkes, R., et al. 1994, Nature, 367, 624
 Brown, P., Marchenko, V., Moser, D. E., Weryk, R., & Cooke, W. 2013, Meteorit. Planet. Sci., 48, 270
 Brown, P., McCausland, P., Fries, M., et al. 2011, Meteorit. Planet. Sci., 46, 339
 Brown, P., Pack, D., Edwards, W., et al. 2004, Meteorit. Planet. Sci., 39, 1781
 Brown, P., Wong, D., Weryk, R., & Wiegert, P. 2010, Icarus, 207, 66
 Brown, P. G., Hildebrand, A. R., Zolensky, M. E., et al. 2000, Science, 290, 320
 Brown, P. G., McCausland, P., Hildebrand, A., et al. 2023, Meteorit. Planet. Sci., 58, 1773
 Brown, P. G., Vida, D., Moser, D., et al. 2019, Meteorit. Planet. Sci., 54, 2027
 Brož, M., Vernazza, P., Marsset, M., et al. 2024a, A&A, 689, A183
 Brož, M., Vernazza, P., Marsset, M., et al. 2024b, Nature, 634, 566
 Carbognani, A. & Fenucci, M. 2023, MNRAS, 525, 1705
 Cephecha, Z. 1961, Bull. astr. Inst. Czechosl., 12, 21
 Chow, I. & Brown, P. G. 2025, Icarus, 429, 116444
 Colas, F., Zanda, B., Bouley, S., et al. 2020, A&A, 644, A53
 de la Fuente Marcos, C. d. & De la Fuente Marcos, R. 2016, MNRAS, 456, 2946
 Devillepoix, H., Cupak, M., Bland, P., et al. 2020, P&SS, 191, 105036
 Devillepoix, H. A., Sansom, E. K., Bland, P. A., et al. 2018, Meteorit. Planet. Sci., 53, 2212
 Devillepoix, H. A. R., Sansom, E. K., Shober, P., et al. 2022, Meteorit. Planet. Sci., 57, 1328
 Drummond, J. D. 1981, Icarus, 45, 545
 Durišová, S., Neslušan, L., Hajduková, M., Rudawska, R., & Jopek, T. 2024, MNRAS, 535, 3661
 Dyl, K. A., Benedix, G. K., Bland, P. A., et al. 2016, Meteorit. Planet. Sci., 51, 596
 Egal, A., Gural, P., Vaubaillon, J., Colas, F., & Thuillot, W. 2017, Icarus, 294, 43
 Egal, A., Vida, D., Colas, F., et al. 2025, Nat. Astron
 Ferus, M., Petera, L., Koukal, J., et al. 2020, Icarus, 341, 113670
 Fry, C., Melanson, D., Samson, C., et al. 2013, Meteorit. Planet. Sci., 48, 1060
 Gardiol, D., Barghini, D., Buzzoni, A., et al. 2021, MNRAS, 501, 1215
 Granvik, M., Morbidelli, A., Jedicke, R., et al. 2016, Nature, 530, 303
 Granvik, M., Morbidelli, A., Jedicke, R., et al. 2018, Icarus, 312, 181
 Granvik, M. & Walsh, K. J. 2024, ApJL, 960, L9
 Gronchi, G. F. & Milani, A. 2001, Icarus, 152, 58
 Halliday, I. 1987, Icarus, 69, 550
 Halliday, I., Blackwell, A. T., & Griffin, A. A. 1978, JRASC, 72, 15
 Halliday, I., Griffin, A. A., & Blackwell, A. T. 1996, Meteorit. Planet. Sci., 31, 185
 Hasegawa, I. 1990, PASJ, 42, 175
 Hlobík, F. & Tóth, J. 2024, Planet. Space Sci., 240, 105827
 Jenniskens, P. 2006, Meteor showers and their parent comets (Cambridge University Press)
 Jenniskens, P. 2008, Icarus, 194, 13
 Jenniskens, P. & Devillepoix, H. A. 2025, Meteorit. Planet. Sci., 60, 928
 Jenniskens, P., Fries, M. D., Yin, Q.-Z., et al. 2012, Science, 338, 1583
 Jenniskens, P., Gabadirwe, M., Yin, Q.-Z., et al. 2021, Meteorit. Planet. Sci., 56, 844
 Jenniskens, P., Jopek, T. J., Rendtel, J., et al. 2009a, WGN, 37, 19
 Jenniskens, P., Moskovitz, N., Garvie, L. A., et al. 2020, Meteorit. Planet. Sci., 55, 535
 Jenniskens, P., Rubin, A. E., Yin, Q.-Z., et al. 2014, Meteorit. Planet. Sci., 49, 1388
 Jenniskens, P., Utas, J., Yin, Q.-Z., et al. 2019, Meteorit. Planet. Sci., 54, 699
 Jenniskens, P. a., Shaddad, M. H., Numan, D., et al. 2009b, Nature, 458, 485
 JeongAhn, Y. & Malhotra, R. 2014, Icarus, 229, 236

Jopek, T. & Froeschlé, C. 1997, *A&A*, 320, 631

Jopek, T., Neslušan, L., Rudawska, R., & Hajduková, M. 2024, *A&A*, 682, A159

Jopek, T., Valsecchi, G., & Froeschlé, C. 1999, *MNRAS*, 304, 751

Jopek, T. J. 1993, *Icarus*, 106, 603

Jopek, T. J. 2020, *MNRAS*, 494, 680

Jopek, T. J. & Bronikowska, M. 2017, *Planet. Space Sci.*, 143, 43

Jopek, T. J., Rudawska, R., & Bartczak, P. 2008, *Earth Moon Planets*, 102, 73

Kartashova, A., Golubaev, A., Mozgova, A., et al. 2020, *P&SS*, 193, 105034

Kholshevnikov, K., Kokhirova, G., Babadzhanov, P., & Khamroev, U. 2016, *MNRAS*, 462, 2275

Kohout, T., Haloda, J., Halodová, P., et al. 2017, *Meteorit. Planet. Sci.*, 52, 1525

Koten, P., Vaubaillon, J., Čapek, D., et al. 2014, *Icarus*, 239, 244

Lauretta, D., Hergenrother, C., Chesley, S., et al. 2019, *Science*, 366

Llorca, J., Trigo-Rodríguez, J. M., Ortiz, J. L., et al. 2005, *Meteorit. Planet. Sci.*, 40, 795

McCrosky, R. E., Posen, A., Schwartz, G., & Shao, C.-Y. 1971, *J. Geophys. Res.*, 76, 4090

McMullan, S., Vida, D., Devillepoix, H. A., et al. 2024, *Meteorit. Planet. Sci.*, 59, 927

Neslušan, L. & Hajduková, M. 2014, *A&A*, 566, A33

Neslušan, L. & Hajduková, M. 2021, *AJ*, 162, 20

Neslušan, L., Kaňuchová, Z., & Tomko, D. 2013, *A&A*, 551, A87

Neslusán, L., Svoren, J., & Porubcan, V. 1998, *A&A*, 331, 411

Pauls, A. & Gladman, B. 2005, *Meteorit. Planet. Sci.*, 40, 1241

Peña-Asensio, E. & Sánchez-Lozano, J. M. 2024, *Adv. Space Res.*, 74, 1073

Peña-Asensio, E., Trigo-Rodríguez, J. M., & Rimola, A. 2022, *AJ*, 164, 76

Pokorný, P. & Vokrouhlický, D. 2013, *Icarus*, 226, 682

Popova, O. P., Jenniskens, P., Emel'yanenko, V., et al. 2013, *Science*, 342, 1069

Reddy, V., Vokrouhlický, D., Bottke, W. F., et al. 2015, *Icarus*, 252, 129

Robitaille, T. P., Tollerud, E. J., Greenfield, P., et al. 2013, *A&A*, 558, A33

Rožek, A., Breiter, S., & Jopek, T. 2011, *MNRAS*, 412, 987

Sansom, E. K., Bland, P. A., Towner, M. C., et al. 2020, *Meteorit. Planet. Sci.*, 55, 2157

Sansom, E. K., Gritsevich, M., Devillepoix, H. A., et al. 2019, *ApJ*, 885, 115

Scott, E. & Herzog, G. 2021, in 52nd LPSC No. 2548, 1833

Sheather, S. J. & Jones, M. C. 1991, *J. R. Stat. Soc.: Series B (Methodological)*, 53, 683

Shober, P. M., Caffee, M. W., & Bland, P. A. 2024, *Meteorit. Planet. Sci.*, n/a

Shober, P. M., Courtot, A., & Vaubaillon, J. 2025a, *A&A*, 693, A23

Shober, P. M., Devillepoix, H. A., Sansom, E. K., et al. 2022, *Meteorit. Planet. Sci.*, 57, 1146

Shober, P. M., Devillepoix, H. A., Vaubaillon, J., et al. 2025b, *Nat. Astron.*, 1

Shober, P. M. & Vaubaillon, J. 2024, *A&A*, 686, A130

Shober, P. M., Vaubaillon, J., Anghel, S., et al. 2023, in Proc. ACM 2023, Lunar and Planetary Institute, Houston, Texas, IPI Contribution No. 2851, Abstract #2402

Šrbený, L., Krzesińska, A. M., Borovička, J., et al. 2022, *Meteorit. Planet. Sci.*, 57, 2108

Southworth, R. & Hawkins, G. 1963, *Smith. Contrib. Astrophys.*, 7, 261

Spurný, P., Borovička, J., Baumgarten, G., et al. 2017, *P&SS*, 143, 192

Spurný, P., Borovička, J., Kac, J., et al. 2010, *Meteorit. Planet. Sci.*, 45, 1392

Spurný, P., Borovička, J., & Šrbený, L. 2020, *Meteorit. Planet. Sci.*, 55, 376

Spurný, P., Borovička, J., Šrbený, L., Hankey, M., & Neubert, R. 2024, *A&A*, 686, A67

Spurný, P., Haloda, J., Borovička, J., Šrbený, L., & Halodová, P. 2014, *A&A*, 570, A39

Spurný, P., Oberst, J., & Heinlein, D. 2003, *Nature*, 423, 151

Steel, D., Asher, D., & Clube, S. 1991, *MNRAS*, 251, 632

Steel, D. I. & Baggaley, W. 1985, *MNRAS*, 212, 817

Svoren, J., Neslusán, L., & Porubcan, V. 1993, *Contrib. Astron. Obs. Skalnaté Pleso*, 23, 23

Turner, S., McGee, L., Humayun, M., Creech, J., & Zanda, B. 2021, *Science*, 371, 164

Unsalan, O., Jenniskens, P., Yin, Q.-Z., et al. 2019, *Meteorit. Planet. Sci.*, 54, 953

Valsecchi, G., Jopek, T., & Froeschlé, C. 1999, *MNRAS*, 304, 743

Vida, D., Brown, P. G., & Campbell-Brown, M. 2017, *Icarus*, 296, 197

Vida, D., Brown, P. G., & Campbell-Brown, M. 2018, *MNRAS*, 479, 4307

Vida, D., Šegon, D., Šegon, M., et al. 2021, Novo Mesto meteorite fall-trajectory, orbit, and fragmentation analysis from optical observations, Tech. rep., Copernicus Meetings

Vokrouhlický, D. & Nesvorný, D. 2008, *AJ*, 136, 280

Wiegert, P., Brown, P., Pokorný, P., et al. 2020, *AJ*, 159, 143

Appendix A: List of the 46 recovered meteorite falls

Table A.1: Instrumentally observed recovered meteorite falls used in this study.

Name	Type	Location	Date	m_{∞} (kg)	m_{found} (kg)	Source
Pribram	H5	Czech Rep.	1959/04/07	<5000	5.56	Ceplecha (1961)
Lost City	H5	USA	1970/01/04	165	17	McCrosky et al. (1971)
Innisfree	L5	Canada	1977/02/06	42	4.58	Halliday et al. (1978)
Benešov	LL3.5, H5	Czech Rep.	1991/05/07	4100	0.01	Spurný et al. (2014)
Peekskill	H6	USA	1992/10/09	<10 000	12.57	Brown et al. (1994)
Tagish Lake	C2-ung.	Canada	2000/01/18	75000	10	Brown et al. (2000)
Moravka	H5	Czech Rep.	2000/05/06	1500	0.63	Borovička & Kalenda (2003)
Neuschwanstein	EL6	Germany	2002/04/06	300	6.19	Spurný et al. (2003)
Park Forest	L5	USA	2003/03/27	11000	18	Brown et al. (2004)
Villalbeto de la Peña	L6	Spain	2004/01/04	760	3.5	Llorca et al. (2005)
Bunburra Rockhole	Eucrite	Australia	2007/07/20	22	0.32	Bland et al. (2009)
Almahata Sitta	Ureilite +other	Sudan	2008/10/07	83000	3.95	Jenniskens et al. (2009b)
Buzzard Coulee	H4	Canada	2008/11/21	15 000	41	Fry et al. (2013)
Maribo	CM2	Denmark	2009/01/17	1500	0.03	Borovička et al. (2019)
Jesenice	L6	Slovenia	2009/04/09	170	3.67	Spurný et al. (2010)
Grimsby	H5	Canada	2009/09/26	33	0.22	Brown et al. (2011)
Kosice	H5	Slovakia	2010/02/28	3500	4.3	Borovička et al. (2013b)
Mason Gully	H5	Australia	2010/04/13	40	0.02	Dyl et al. (2016)
Križevci	H6	Croatia	2011/02/04	25-100	0.29	Borovička et al. (2015b)
Sutter's Mill	C, CM2	USA	2012/04/22	50000	0.99	Jenniskens et al. (2012)
Novato	L6	USA	2012/10/18	80	0.31	Jenniskens et al. (2014)
Chelyabinsk	LL5	Russia	2013/02/15	1 200 000	~1000	Popova et al. (2013)
Annama	H5	Russia	2014/04/18	472	0.17	Kohout et al. (2017)
Žďár nad Sázavou	L3	Czech Rep.	2014/12/09	170	0.05	Spurný et al. (2020)
Porangaba	L4	Brazil	2015/01/09	0.976	0.976	Ferus et al. (2020)
Sarıçık	Howardite	Turkey	2015/09/02	6000 - 20000	15.24	Unsalan et al. (2019)
Creston	L6	USA	2015/10/24	10-100	0.688	Jenniskens et al. (2019)
Murrili	H5	Australia	2015/10/27	37.9±2.3	1.68	Sansom et al. (2020)
Ejby	H5/6	Denmark	2016/02/06	250	8.94	Spurný et al. (2017)
Dishchii'bikoh	LL7	USA	2016/06/02	3000-15000	0.0795	Jenniskens et al. (2020)
Dingle Dell	L/LL5	Australia	2016/10/31	40	1.15	Devillepoix et al. (2018)
Hamburg	H4	USA	2018/01/17	60 - 225	1	Brown et al. (2019)
Motopi Pan	Howardite	Botswana	2018/06/02	5500	0.214	Jenniskens et al. (2021)
Ozerki	L6	Russia	2018/06/21	94000±20000	6.5	Kartashova et al. (2020)
Arpu Kuilpu	H5	Australia	2019/06/01	0.91	0.031	Shober et al. (2022)
Flensburg	C1-ungr.	Germany	2019/09/12	10000-20000	0.0245	Borovička et al. (2021)
Cavezzo	L5-an	Italy	2020/01/01	3.5	0.055	Gardioli et al. (2021)
Novo Mesto	L5	Slovenia	2020/02/28	470	0.72	Vida et al. (2021)
Madura Cave	L5	Australia	2020/06/19	30-60	1.072	Devillepoix et al. (2022)
Narashino	H5	Japan	2020/07/02		0.35	Metbull
Traspena	L5	Spain	2021/01/18	2620	0.527	Andrade et al. (2023)
Winchcombe	CM2	UK	2021/02/28	12.5	0.602	McMullan et al. (2024)
Antonin	L5	Poland	2021/07/15	50-500	0.35	Šrbený et al. (2022)
Golden	L/LL5	Canada	2021/10/04	70	2.2	Brown et al. (2023)
Saint-Pierre-le-Viger	L5-6	France	2023/02/13	780	1.2	Egal et al. (2025)
Ribbeck	Aubrite	Germany	2024/01/24	140	1.8	Spurný et al. (2024)